

Strains Due to Coupled Phenomena – Particle-level Analyses

Dante Fratta

University of Wisconsin-Madison. Madison, WI 53706. USA

J. Carlos Santamarina

Georgia Institute of Technology. Atlanta, GA 30332. USA

ABSTRACT: The interaction between the solid particles and the pore fluid in granular materials affects various interparticle forces. The change in any one of these forces triggers the response of the granular skeleton, causes strain and even important fabric changes. Coupling phenomena that result in skeletal strains are related to fluid properties, electrical-chemical interactions, and thermal effects. The relevance of such couplings increases as the particle size d and the effective skeletal confinement σ' decrease, and well-defined coupling regions can be defined in the d - σ' space. Experimental results support order-of-magnitude estimates based on particle-level analyses.

1 INTRODUCTION

Hooke's law predicts the strain induced by a change in the state of the stress (Sokolnikoff 1956; Heyman 1972). In the case of poroelastic media, such as granular materials, strains result from changes in the pore fluid pressure as well as changes in the stress carried by the skeleton (Biot 1941; Scott 1963; Terzaghi and Peck 1967). Furthermore, in some granular materials, strains also result from changes in electrical, chemical and thermal conditions (Casagrande 1948; Ikeda 1990; Mitchell 1991).

These forms of energy coupling are macroscale-compatible with fundamental physical principles, in particular energy conservation and Le Châtelier's Principle (a system in equilibrium will oppose any disturbance). When energy coupling phenomena are analyzed at the particle-level, the essential nature of material behavior becomes apparent, and the magnitude of energy coupling parameters characterizes the medium and the physical processes that govern it.

Energy coupling effects are repeatable when low-energy input excitations are applied; for example, a small-strain mechanical excitation is accompanied by elasto→electrical coupling (e.g., seismoelectricity – Thompson 1936; Pride 1994; Santamarina and Fratta 2003), elasto→thermal coupling (e.g., thermoelasticity – Luong 1996) and elasto→chemical coupling (local ion displacement – Thompson and Gist 1993).

Severe non-linear energy coupling effects may also develop in particulate materials; coupling-

induced strain often falls in this category. In order to understand the development of non-linear coupling, the fundamental nature of particulate materials must be uncovered first. This study starts with a review of particle-level forces; then, the microscale impact of changes in electrical and chemical conditions and the ensuing strains are analyzed.

2 PARTICLE-LEVEL FORCES

Soils involve mineral grains forming a porous skeleton. The interconnected pores are filled with fluid, e.g., air, water, organics, or a mixture. All these phases (i.e., solid, liquid, and gas), not only interact through skeletal forces but also through hydrodynamic forces, capillarity forces, and electrical forces (details in Santamarina 2002).

Skeletal Forces. A boundary effective stress σ' [Pa] acting on a random packing of spheres with void ratio e [] will cause an average normal contact force \underline{F}_{ske} [N],

$$\underline{F}_{ske} = \sigma' d^2 \left[\frac{\pi(1+e)}{12} \right] \quad \text{for } 0.4 < e < 1.0 \quad (1)$$

where d [m] is the particle diameter. However the distribution of normal contact forces is not uniform: some particles align into load-carrying columns to support the applied boundary stresses while other particles provide confinement to prevent buckling in the columnar formation.

Hydrostatic forces. The presence of a continuous water phase within the granular skeleton gives rise to hydrostatic stress u , increases the total stress σ , and reduces both the effective stress $\sigma' = \sigma - u$ in the soil mass and the normal contact forces F_{ske} between particles (Equation 1).

Hydrodynamic forces. The movement of viscous fluids through soil pores results on a velocity gradient and the generation of shear stress and drag forces F_{drag} against grains. For laminar flow:

$$F_{drag} = 3\pi\mu v d \quad \text{Stokes' equation} \quad (2)$$

where μ [Pa·s] is the viscosity of the fluid and v [m/s] is the relative particle-fluid velocity. The relative average velocity in a soil mass may be expressed in terms of the hydraulic conductivity of the soil k [m/s], the hydraulic gradient i_h [], and porosity $n = e/(1+e)$ []:

$$v = \frac{ki_h}{n} \quad (3)$$

Drag forces act on the soil skeleton and change the normal forces F_{ske} (hence, σ' as per Equation 1).

Capillarity forces. Two immiscible fluids (e.g., air and electrolyte in unsaturated soils) gives rise to surface tension T_s [Pa·m]. The surrounded fluid develops a fluid pressure u :

$$u = T_s \left(\frac{1}{r_1} + \frac{1}{r_2} \right) \quad \text{Laplace's equation} \quad (4)$$

where r_1 and r_2 [m] are curvature radii. In most cases, minerals are hydrophilic and the liquid electrolyte tends to wet the surface of the solid particles, as shown in Figure 1.

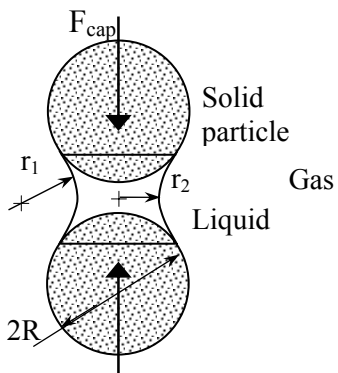


Figure 1: Definition of radii in Laplace's equation.

As the soil dries, the liquid phase hangs to the particle and suction develops, effectively contributing a normal force between particles (asymptotic value):

$$F_{cap} = \frac{\pi d^2 u}{4} \quad (5)$$

van der Waals attraction between two particles at a distance t [m] apart is

$$F_{att} = \frac{A_h d^2}{24t^3} \quad (6)$$

where A_h [=0.64·10⁻²⁰ J for silica-water-silica and 0.09·10⁻²⁰ J for silica-CCl₄-silica] is the Hamaker constant (Lyklema 1995; Israelachvili 1992).

Electrical repulsion. Mineral soil particles and electrolytes interact. Under normal pH conditions, the mineral surface exhibits negative surface charge due to uncompensated charges at the surface and isomorphous substitution. Due to these surface negative charges, hydrated cations are attracted and hydrated anions are repelled. The balance between electrical forces among charges and thermal agitation cause a particular charge distribution in the vicinity of particles (Figure 2).

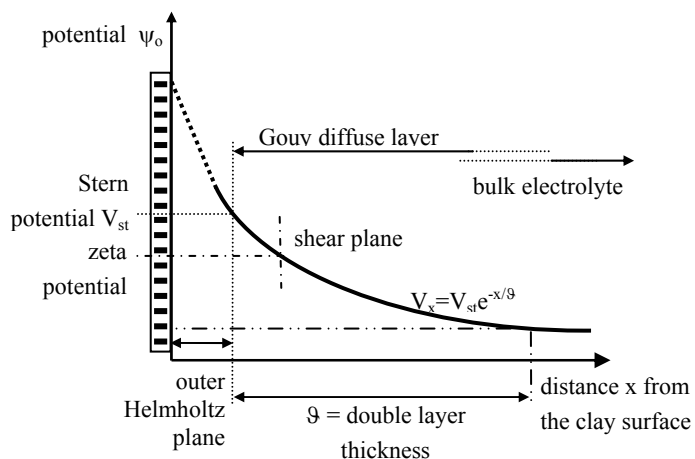


Figure 2: Double layer at a mineral-electrolyte interface. The double layer thickness θ is the distance where the potential drops to V_{st}/e . Ions outside the shear plane move with the bulk electrolyte.

The distance between the outer Helmholtz plane and the point where Stern potential drops to V_{st}/e is known as the “thickness of the double layer” or Debye-Huckel length:

$$\theta = \sqrt{\frac{\kappa' \epsilon_0 RT}{2c_0 z^2 F^2}} \quad (7)$$

where κ' [] is real relative permittivity of the pore fluid, ϵ_0 [=8.85·10⁻¹² F/m] is the permittivity of the free space, R [=8.8315 J mol⁻¹ K⁻¹] is the gas constant, T [K] is the temperature, c_0 [mol L⁻¹] is the ionic concentration of the electrolyte, z [] is the valence of the prevailing ion, and F [=96485.3 C mol⁻¹] is the Faraday's constant. When the pore fluid moves relative to the particle, part of the ionic cloud moves with the fluid; for simplicity, a sharp shear plane is often assumed. The potential on the shear plane is the zeta-potential ζ .

Equation 7 shows the interaction of thermal and electrical phenomena at the liquid-solid mineral inter-phase. The interaction between neighbor particles and their diffuse double layers develop non-linear attraction and repulsion forces:

$$F_{\text{rep}} = 16\pi RTc_0 d^2 9e^{-\frac{t}{\vartheta}} \quad (8)$$

Figure 3 shows the combined effects of electrical repulsion and the van der Waals' attraction.

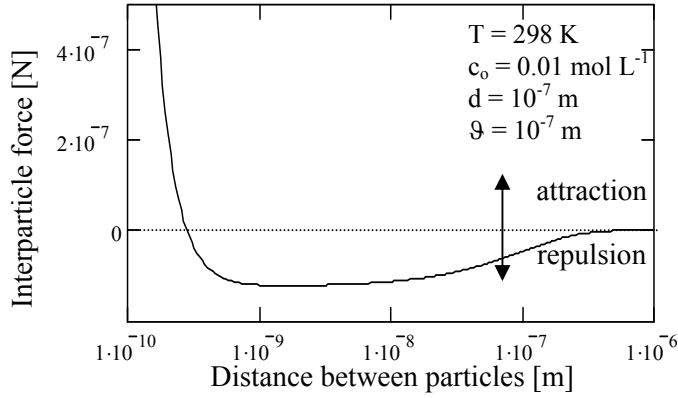


Figure 3: Electrical repulsion and van der Waals' attraction.

Soil behavior regimes. Figure 4 shows a comparative analysis of particle-level forces vs. particle size. The possibility for coupling-induced strains increases when particle level forces of capillary and electrical nature gain relevance relative to particle self weight and skeletal forces. Therefore, coupling induced strains should be expected in micron and sub-micron particles subjected to low confinement.

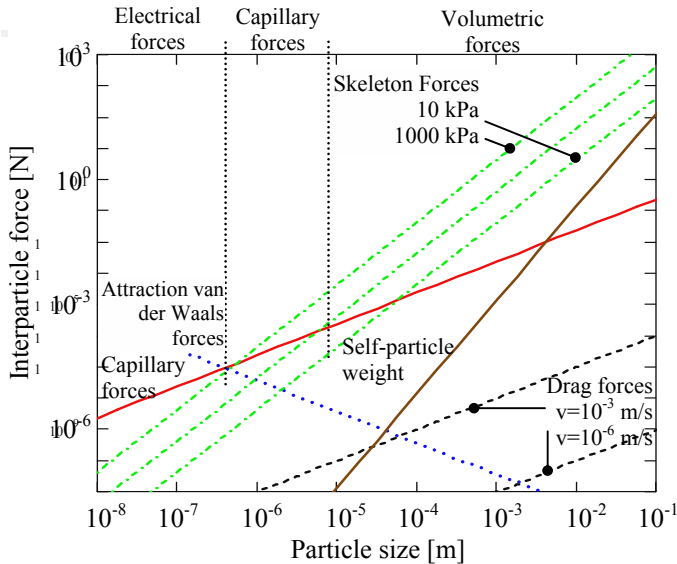


Figure 4: Comparison of interparticle forces versus particle size. For a given particle diameter, the higher the force, the more relevant the force is in controlling the behavior of the particulate medium (van der Waals force computed for particle separation $t=0.002 d$ - Figure after Santamarina 2002).

Ionic diffusion reflects the random vibration of thermally activated charges. It takes place throughout the pore fluid and also leads to the exchange of ions in the diffuse layer around mineral particles. The increase in ionic concentration in the pore fluid does not alter the interparticle van der Waals attraction significantly (the Hamaker constant is little affected by the ionic concentration). However, electrical repulsion decreases as the ionic concentration increases, and the van der Waals attraction increases as the separation between particles decreases. At high ionic concentration, the repulsion well is overcome and particles tend to aggregate. The shrinkage strain associated to the increase in ionic concentration transfers skeletal load onto the pore water, the fluid pressure increases near the diffusion front, and water migrates away.

The volumetric strain induced by chemical changes in soils may be estimated assuming that the change in effective stress is the change in electrical forces or in osmotic pressure $\Delta\sigma' = \Delta\Pi$.

$$\varepsilon_v = \varepsilon_1 + \varepsilon_2 + \varepsilon_3 = B \cdot \Delta\Pi \quad (9)$$

where B is the bulk modulus of the soil skeleton. The time rate of the volumetric strain depends both on the consolidation coefficient and on the chemical diffusion coefficient. Typical values of consolidation and chemical diffusion coefficients are presented in Table 1.

Table 1: Chemical and pressure diffusion coefficients for kaolinite and bentonite clays, and common ions and salts (Mitchell 1993).

Clay and Ions	Chemical Diffusion Coefficient D [$\text{m}^2 \text{s}^{-1}$]	Pressure diffusion Coefficient C_v [$\text{m}^2 \text{s}^{-1}$]
Kaolinite	$\approx 3 \cdot 10^{-10}$	$\approx 5 \cdot 10^{-7}$
Bentonite	$\approx 5 \cdot 10^{-10}$	$\approx 1 \cdot 10^{-9}$

Notes: The chemical diffusion coefficient ranges from $2 \cdot 10^{-10}$ to $2 \cdot 10^{-9}$ m^2/s for most chemicals in most saturated soils.

The addition of a high ionic concentration fluid at the boundary of a granular skeleton (concentration greater than the pore fluid) causes two effects. First, water in the pore fluid tends to migrate from the soil towards the high concentration pore fluid at the boundary due to the soil response as a semi-permeable membrane. Second, ions diffuse into the soil and cause a reduction in interparticle electrical repulsion, the granular skeleton shrinks and water is expelled. The interplay between these two parallel processes (and their corresponding rates) manifests in complex macroscale response. Consider the following example (Figure 5 - Pore fluid pressure is measured at the bottom of the specimen):

- A mixture of bentonite and deionized water is consolidated to a vertical stress $\sigma'_v=100$ kPa.
- A KCl electrolyte solution $c_{final}=4.0$ M is added at the top to the specimen through a porous stone.
- Osmotic negative pore fluid pressure builds up first, as soon as the diffusion front traverses the porous stone ($t\sim 7$ min).
- As ions diffuse into the bentonite specimen, they enter the double layer, reduce electrical repulsion forces, and the pore fluid temporarily picks up part of the skeletal force (positive pore fluid pressure) until it has enough time for pressure diffusion. The time scale is estimated as

$$t_{90} = \frac{T_{90} \cdot H_{dsoil}^2}{D_{KCl}} = \frac{0.848 \cdot (0.02m)^2}{19.9 \cdot 10^{-10} \frac{m^2}{s}} = 2841 \text{ min} \quad (10)$$

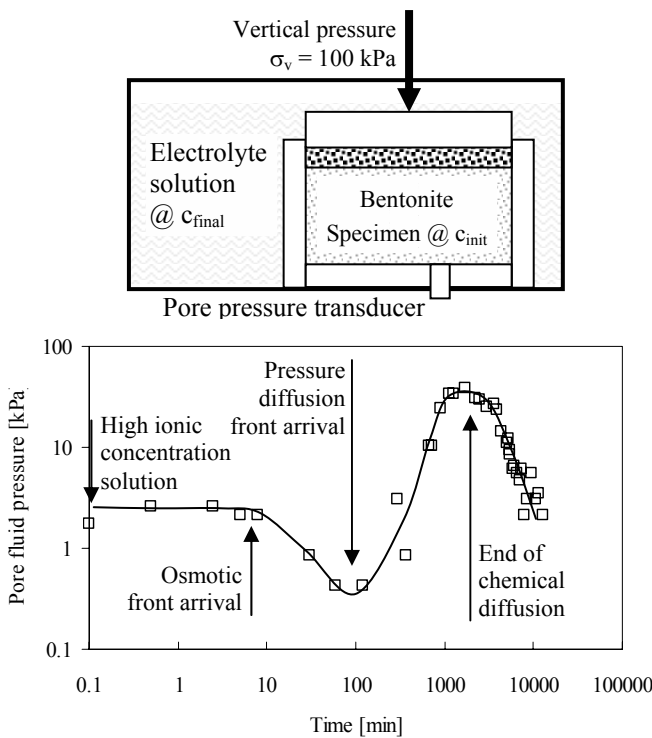


Figure 5: Pore pressure generation due to the chemical diffusion of a high ionic concentration KCl solution ($c_{final}=4.0$ M) through a bentonite-water mixture ($c_{init}=0$ M). Data re-analyzed from Santamarina and Fam (1995).

4 STRAINS FROM ELECTRICAL CHANGES

An externally imposed electric field adds to the electric field created by ionic charges and surface charged clay particles. The externally applied field does not have a significant effect on interparticle electrical forces. Still, an externally applied DC electric field promotes the migration of hydrated ions. The sequence of events leading to fluid flow and consolidation is complex, and often includes co-existing opposite trends. The salient processes are:

- Ions migrate in the soil while electrons flow in the external electric circuit that is used to apply the

field. The accumulation of ions at the interface is known as electrode polarization and causes a high voltage drop at the interface (Klein and Santamarina 1997). Current is maintained by oxidation-reduction and other electrode processes.

- Hydroxyls OH^- migrate from the anode to the cathode, while hydrogen H^+ does otherwise. The mobility of $H^+=32.6 \cdot 10^{-8} [m^2V^{-1}s^{-1}]$ is higher than the mobility of $OH^-=20.5 \cdot 10^{-8} [m^2V^{-1}s^{-1}]$, and H^+ advances through the soil at a faster rate leaving behind a large region with high pH. At extreme pH conditions, the mineral experiences dissolution (Chorover and Sposito 1995; Malengrau and Sposito 1996).
- If the soil has no excess salts, the pore fluid is deionized water. When the external electric field is applied, hydrated counterions in the diffuse layer near the mineral surface migrate from one particle to the next if continuity is supported at electrodes and drag water with them. This effect is independent of the pore thickness (Helmholtz-Smoluchowski theory - Mitchell 1993; Klein and Santamarina, 2003).
- If the soil has excess salts, the pore fluid is an electrolyte and additional transport takes place. In this case as hydrated cations move towards the cathode and hydrated anions to the anode, they carry different number of hydrating water molecules, which is related to the field intensity on the periphery of ions (the number of hydrating water molecules is higher for the common cations than for anions - Figure 6). Therefore, more water migrates towards the cathode than towards the anode.

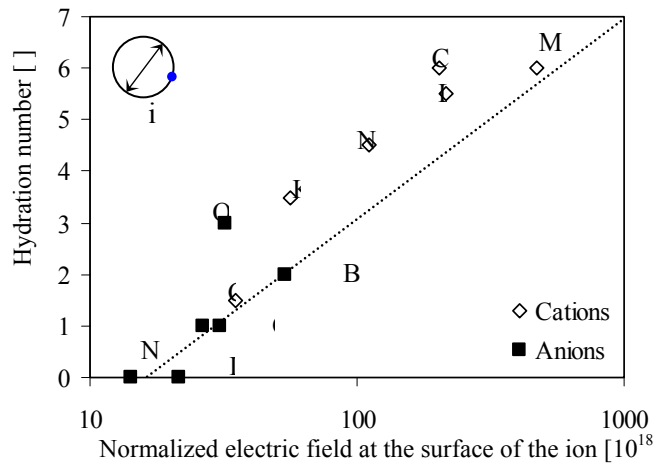


Figure 6 The number of hydrating molecules as a function of ion size and valence z/r^2 . Notice that common cations involve a larger number of hydrating water molecules than anions (ion data are tabulated in Israechlavili, 1992).

- The pore between particles is considered small when the interparticle distance is less than twice the Debye-Huckel length but greater than twice the distance to the shear plane. This size pores act as semi-permeable membranes, excluding co-ions

(same charge as clay surface), and allowing counter-ions to exchange and migrate along. When the pH of the medium decreases and goes across the isoelectric point of the mineral, the surface charge density changes from negative to positive and the medium changes from anion-exclusion to cation exclusion. This may cause electroosmotic flow reversal (see Eykholt and Daniel 1994).

- If zero-flow conditions are imposed at the electrodes, the water content and pore pressure increase at the cathode and decrease towards the anode. However, if constant fluid pressure conditions are imposed at the electrodes, then the pore fluid pressure depression develops between electrodes (see Eykholt and Daniel 1994; Eykholt 1997). The effective stress increases where the pore fluid pressure decreases. The volume reduction of the soil towards the anode depends on the soil skeletal stiffness.

The effectiveness of hydrated ion migration is related to the hydraulic conductivity of the soil, which in turn decreases as the specific surface S_s [m^2g^{-1}] of the soil increases and the water content w [%] decreases. Larger pores become increasingly less effective at co-ion exclusion, lead to higher hydraulic conductivity and ease counter fluid flow.

- In the meantime, excess ions (not the counterions needed to neutralize the mineral surface charge) have migrated leaving behind a pore fluid with lower ionic concentration.
- Electro-osmotic flow is opposed by the coupled counter gradients that develop, including hydraulic, thermal and chemical gradients. Therefore, while there may be ionic flow when the external field is applied, any depletion/accumulation of pore fluid at the electrodes will be readily cancelled by counter-flow due to hydraulic gradients, hindering electroosmotic consolidation.
- The distinct migration of water, ions, protons and hydroxyls across the medium leaves a non uniform material between electrodes, with spatially varying pore pressure, effective stress, water content, hydraulic conductivity, ionic concentration, electrical conductivity and electric field. Therefore, homogeneous 1-D models must be modified to analyze experimental data (Eykholt and Daniel 1994).
- Pore pressure depression due to water migration increases the effective stress. This effect coexists with the changes in double layer (due to the decrease in ionic concentration) and the change in surface potential during the migration of the acid and basic fronts. The combined effect of all these changes causes a strain in the soil skeleton which is in turn inversely proportional to the stiffness of the skeleton.

A study was performed on kaolinite specimens. It was designed to (1) have similar initial fabric and stiffness prior to chemical diffusion, and (2) preserve general material characteristics except for ionic concentration. Results for two specimens are shown in Figure 7.

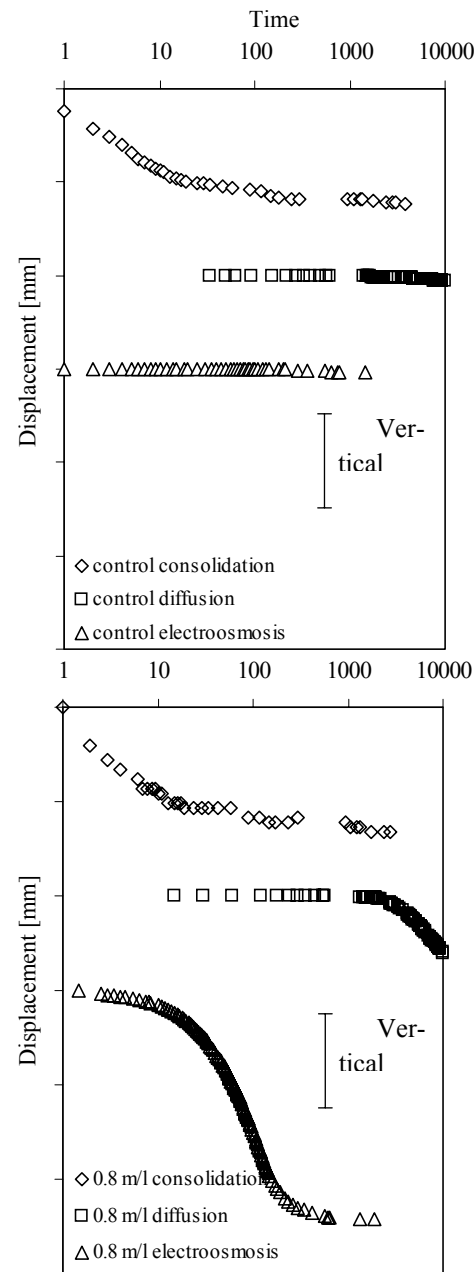


Figure 7: Displacement vs. time during consolidation (from 67.4 kPa to 135 kPa), chemical diffusion and electroosmosis. Kaolinite specimens - data gathered by S. McMechan.

Both specimens were prepared with deionized water and consolidated in an oedometer cell to 135 kPa. The control specimen is kept saturated with deionized water under load, while the other specimen is diffused with a 0.8 mol/l NaCl solution. Finally, both specimens are subjected to an electric field. Figure 8 shows displacement versus time, for each of the three stages: pressure diffusion, chemo-mechanical coupling (chemoosmosis) and electro-mechanical coupling (electroosmosis). The control

specimen exhibits no deformation during electroosmosis, while the specimen diffused with the 0.8 mol/l NaCl solution shows a marked deformation during both chemical diffusion (as predicted in the previous section) and during electroosmosis. The displacement of ions during electroosmosis was monitored by measuring the electrical current (Figure 8). The control specimen shows a very small electrical current confirming the low ionic concentration; furthermore, the current drops as the few present ions are depleted. The specimen diffused with the 0.8 mol/l solution shows a much larger current and the current sharply increases while the specimen consolidates and hydrated ions are removed at a higher rate (around 20 minutes in the electroosmosis process).

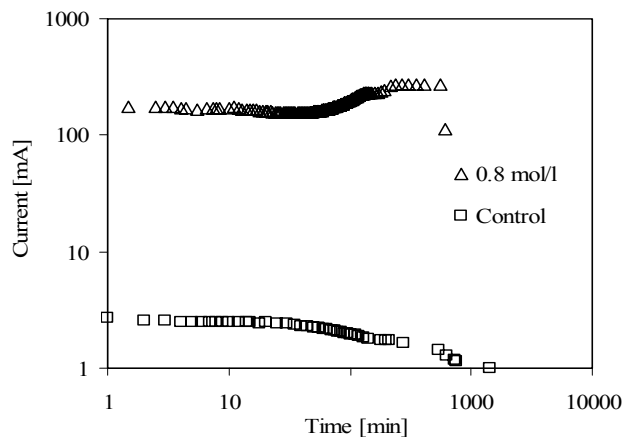


Figure 8: Current vs. time during the electroosmosis.

5 ACKNOWLEDGMENTS

The authors are thankful to Sandra McMechan and Dr. Moheb A. Fam for experimental data. Support was provided by the National Science Foundation.

6 REFERENCES

Barbour, S. L. and Fredlund, D. G. 1989. Mechanisms of Osmotic Flow and Volume Change in Clay Soils. *Canadian Geotechnical Journal* 26: 551-562.

Biot, M. A. 1941. General Theory of Three-Dimensional Consolidation, *Journal of Applied Physics* 12: 155-164.

Casagrande, L. 1948. Electroosmosis in Soils. *Geotechnique*, 1: 159-177.

Casagrande, L. 1983. Stabilization of Soils by Means of Electro-osmosis State of the Art. *Journal of the Boston Engineering Society*, 69: 225-302.

Chorover, J. and Sposito, G. 1995. Dissolution Behavior of Kaolinitic Tropical Soils. *Geochimica et Cosmochimica Acta* 59(15): 3109-3121.

Eykholt, G. R. and Daniel, D. E. 1994. Impact of System Chemistry on Electroosmosis in Contaminated Soil. *Journal of Geotechnical Engineering* 120(5): 797-815.

Eykholt, G. R. 1997. Development of Pore Pressures by Non-Uniform Electroosmosis in Clay". *Journal of Hazardous Materials*, 55, 171-186.

Heyman, J. 1972. *Coulomb's Memoir on Statics*. Imperial College Press, 211 pages.

Ikeda, T. 1990. *Fundamentals of Piezoelectricity*. Oxford Univeristy. Press. Oxford. 263 pages.

Israelachvili, J. 1992. *Intermolecular and Surface Forces*, Second Edition, Academic Press. London, 460 pages.

Klein, K. and Santamarina, J.C. 1997. Broad Band Frequency Measurements with Electromagnetic Waves. *ASTM Geotechnical Testing Journal* 20(2): 168-178.

Klein, K. and Santamarina J. C. 2003. Electrical Conductivity In Soils: Underlying Phenomena. *Journal of Environmental Engineering Geophysics*. 8(4): 263-273.

Loung, M. P. 1986. Characteristics Threshold and Infrared Vibrothermography of Sand. *Geotechnical Testing Journal* 9(2): 80-86.

Lyklema, J. 1995. *Fundamentals of Interface and Colloid Science*, Volume II: Solid and Liquid Interfaces, Academic Press, London.

Malengrau, N. and Sposito, G. 1996. Short-Time Dissolution Mechanisms of Kaolinitic Tropical Soils. *Geochimica et Cosmochimica Acta* 61(20), 4297-4307.

Mitchell, J. K. 1991. Conduction Phenomena: from Theory to Geotechnical Practice. *Geotechnique* 41, 299-340.

Mitchell, J. K. 1993. *Fundamentals of Soil Behavior*, John Wiley and Sons, 437 pages.

Pride, S. R. 1994. Governing Equations for the Coupled Electromagnetic and Acoustic of Porous Media. *Physical Review B* 15: 15678-15696.

Santamarina, J. C. and Fam, M. 1995. Changes in Dielectric Permittivity and Shear Wave Velocity during Concentration Diffusion. *Canadian Geotechnical Journal* 32(4): 647-659.

Santamarina, J. C. and Fratta, D. 2003. Dynamic Electrical-Mechanical Energy Coupling In Electrolyte-Mineral Systems. *Transport in Porous Media* 50(1/2): 153-178.

Santamarina, J. C., Klein, K. A., and Fam, M. A. 2001. *Soils and Waves*. John Wiley & Sons. Chichester. 488 pages.

Santamarina, J. C. 2002. Soil Behavior at the Microscale: Particle Forces, *Soil Behavior and Soft Ground Construction*, ASCE SP#119, pp. 25-56.

Scott, R. F. 1963. *Principles of Soil Mechanics*. Addison-Wesley Publishing Co., Reading, MA, 550 pages.

Sokolnikoff, I. S. 1956. *Mathematical Theory of Elasticity*. Robert E. Krieger Publishing Co., Malabar, FL, 476 pages.

Terzaghi, K. and Peck, R. B. 1967. *Soil Mechanics in Engineering Practice*. John Wiley and Sons, New York, 729 pages.

Thompson, A. H. and Gist, G. A. 1993. Geophysical Applications of Electrokinetic Conversion. *The Leading Edge*, December, 1169-117

Thompson, R. 1936. The Seismic Electric Effect. *Geophysics* 1: 327-335.